catalysts

MDPI

Article

Effect of Calcination Conditions on Co_3O_4 Catalysts in the Total Oxidation of Toluene and Propane

Weidong Zhang [1,2], Claude Descorme [2], Jose Luis Valverde [3] and Anne Giroir-Fendler [2,*]

[1] School of Chemistry and Chemical Engineering, Anhui Province Key Laboratory of Coal Clean Conversion and High Valued Utilization, Anhui University of Technology, Ma'anshan 243002, China; weidong.zhang@ahut.edu.cn
[2] University Lyon, Université Claude Bernard Lyon 1, CNRS, IRCELYON, 2 Avenue Albert Einstein, F-69622 Villeurbanne, France; claude.descorme@free.fr
[3] Faculty of Chemical Science and Technology, University of Castilla-La Mancha, Avenida Camilo José Cela 12, 13005 Ciudad Real, Spain; joseluis.valverde@uclm.es
* Correspondence: anne.giroir-fendler@ircelyon.univ-lyon1.fr

Abstract: Co_3O_4 catalysts were prepared via carbonate precipitation and subsequent calcination under specific conditions. The different catalysts were characterized as received using several techniques and tested in the total oxidation of toluene or propane. Calcination at low temperature or under dynamic conditions resulted in Co_3O_4 catalysts with small crystallite sizes and large surface areas. The performances of the Co_3O_4 catalysts appeared to be closely related to the low-temperature reducibility. The best catalyst, Co-350D, showed a toluene oxidation rate of 44.5 nmol g^{-1} s^{-1} at 200 °C and a propane oxidation rate of 54.0 nmol g^{-1} s^{-1} at 150 °C. Meanwhile, Co-350D exhibited excellent cycling stability and decent long-term durability in both reactions.

Keywords: volatile organic compounds; Co_3O_4; calcination; toluene oxidation; propane oxidation

check for updates

Citation: Zhang, W.; Descorme, C.; Valverde, J.L.; Giroir-Fendler, A. Effect of Calcination Conditions on Co_3O_4 Catalysts in the Total Oxidation of Toluene and Propane. *Catalysts* **2023**, *13*, 992. https://doi.org/10.3390/catal13060992

Academic Editor: Hongxing Dai

Received: 18 May 2023
Revised: 6 June 2023
Accepted: 7 June 2023
Published: 9 June 2023

Copyright: © 2023 by the authors. Licensee MDPI, Basel, Switzerland. This article is an open access article distributed under the terms and conditions of the Creative Commons Attribution (CC BY) license (https://creativecommons.org/licenses/by/4.0/).

1. Introduction

Volatile organic compounds (VOCs), emitted from industrial manufacturing, automobile vehicles, and domestic activities and involved in the formation of ozone, photochemical smog, and secondary aerosols, are major contributors to air pollution [1]. Some of them are identified to be carcinogenic, teratogenic, and mutagenic, threatening human health [1]. Converting VOCs to harmless CO_2 and H_2O by catalytic oxidation is one of the most promising solutions. As the leading catalysts in the catalytic oxidation of VOCs, noble metals have been widely studied in the last decades [2]. However, viewing from an economic and sustainable perspective, transition metal oxides that exhibit comparable activity to noble metals could be a better choice. Among transition metal oxides, Co_3O_4 nanocatalysts have been proven to be very active in the total oxidation of toluene [3–11] and propane [12–20], two representative model VOCs. According to the well-accepted redox reaction mechanisms [21], the activity of Co_3O_4 is mainly governed by its reducibility and oxygen mobility, and these redox properties are generally related to the crystallite size, strain, structural defects, and surface cobalt oxidation state of Co_3O_4. Rational design and control of these properties lie in the preparation process. Precipitation is a commonly used method for Co_3O_4 synthesis with the advantages of simple steps, easy operation, and industrial scalability. The variation of precipitation conditions, such as precipitation agent [22], precipitation pH [23], or calcination procedure [24,25] could affect the physicochemical properties of Co_3O_4 and, consequently, the catalytic performance.

Recently, we have investigated the effect of the precipitation agent on Co_3O_4 catalysts in the total oxidation of toluene and propane and demonstrated carbonate as the most promising agent [26]. Straight after, we further singled out the optimum precipitation pH, 9.5 [27]. In addition to these, calcination conditions may be another important

parameter that affects the physicochemical properties and catalytic performance of the catalysts. For instance, low calcination temperatures can be beneficial for obtaining small crystallite sizes and facilely accessible active sites [24,25]. By adjusting the calcination temperature, the spin states of Co^{3+} in $LaCoO_3$ catalysts can be accordingly tuned, which in turn determines the catalytic activity [28]. The content of surface oxygen vacancies in Co_3O_4/SiO_2 catalysts prepared via impregnation can be controlled by calcinating at various temperatures [29]. High temperature calcination oxidized excess surface Co^{2+} and lowered surface oxygen vacancies concentration. Shen et al. prepared Co_3O_4 by a solvothermal method and engineered the bond strength of Co–O in Co_3O_4 catalysts by annealing at 270, 300, 350, and 400 °C, respectively [3]. It was demonstrated that Co_3O_4 annealed at 300 °C exhibited the weakest Co–O strength, the highest surface oxygen species activity, and thus the best toluene oxidation performance. Wang et al. modulated oxygen vacancies in Co_3O_4 by controlling the calcination temperature (200–450 °C) [30]. The catalyst prepared via a hydrothermal method followed by calcination at 200 °C gave the best propane oxidation performance due to the abundance of oxygen defects. Liu et al. investigated the structural changes of CuO_x-CoO_y-CeO_2 ternary oxides in the calcination temperature range of 400 to 800 °C [31]. When calcined at 600 °C, the surface enrichment of Cu^+, the improved interaction between Co_3O_4 and CeO_2, and the increased oxygen vacancies in CeO_2 were simultaneously achieved, giving the highest CO oxidation activity. Wu et al. found that calcination of $CoCeO_x$ composites at high temperature resulted in much larger Co_3O_4 crystallites, lower surface areas, decreased reducibility, fewer surface cobalt species, and decreased amount of acid sites, and in turn inferior methane oxidation activity [32]. Li et al. synthesized Co_3O_4/CeO_2 composites by a modified citrate sol–gel method, in which the catalyst precursors were thermally treated with nitrogen first before calcination in air [33]. The results showed that the nitrogen-air two step annealing contributed to smaller grain size and higher surface area of Co_3O_4/CeO_2, and thereby better methane combustion performance. In addition, calcining in dynamic air is reported to eliminate excess reaction heat, avoiding hot spots and crystal sintering [34].

In this study, four Co_3O_4 catalysts were synthesized using the carbonate-precipitation method at a pH of 9.5, by varying the calcination temperature (350 °C vs. 550 °C) and calcination condition (static air vs dynamic air), to tune the structural and surface properties of the Co_3O_4 materials. The as-prepared catalysts were evaluated in the total oxidation of toluene and propane. Several characterization techniques were applied to probe the determining factor of the catalytic activity.

2. Results and Discussion

2.1. Structural and Textural Characterization

Figure S1 shows TG curve of the cobalt precursor in air flow. The small weight loss from 25 to 150 °C was attributed to the removal of physically adsorbed and chemically combined water. The large weight loss from 150 to 350 °C was due to the transformation of cobalt precursor into Co_3O_4. The slight gradual weight loss above 350 °C may arise from the perfection of the Co_3O_4 crystal. Based on the TG analysis, the cobalt precursor was calcined at 350 °C to produce Co_3O_4 with defective structure, and at 550 °C to generate Co_3O_4 with high crystallinity.

Figure S2 presents the FTIR spectra of the cobalt precursor and the cobalt oxide product. For the cobalt precursor, the broad band at 3495 cm^{-1} was assigned to the stretching and bending modes of the H_2O and O–H groups [35–37]. The bands aroused by carbonate anions occurred at 1390 ($\nu(OCO_2)$, $\nu(CO_3)$), 1070 (ν(C=O)), 829 ($\delta(CO_3)$), 735 (δ(OCO)), and 679 cm^{-1} (ρ(OCO)) [35–37]. The bands at 954 and 512 cm^{-1} were attributed to δ(Co–OH) and ρ_w(Co–OH) [35–37]. After calcination, two bands typical for Co_3O_4 presented at 656 and 545 cm^{-1} [38], accompanied by the disappearance of characteristic bands of cobalt carbonate hydroxide.

The chemical composition of the catalysts is listed in Table 1. The cobalt mass ratios of all catalysts were identical, close to that of stoichiometric Co_3O_4 (73.4 wt.%). The amounts

of residual sodium in all catalysts were similar and were below 0.2 wt.%, thus excluding the possible poisoning effect of sodium on the catalysts [27].

Table 1. Chemical composition, average crystallite size, and textural data of the Co_3O_4 catalysts calcined under different conditions.

Catalysts	Co wt.% [a]	Na wt.% [a]	d (nm) [b]	a (Å) [b]	Strain (%) [b]	S_{geo} (m^2 g^{-1}) [c]	SSA (m^2 g^{-1}) [d]	V_{pore} (cm^3 g^{-1}) [d]
Co-350S	72.7	0.12	16	8.088	0.58	64	61	0.281
Co-350D	72.2	0.11	12	8.090	0.74	81	81	0.365
Co-550S	73.9	0.17	51	8.085	0.17	19	20	0.032
Co-550D	73.3	0.11	29	8.086	0.33	34	33	0.116

[a] Chemical composition determined by ICP-OES. [b] Average crystallite size(d), lattice constant(a) and strain estimated from XRD. [c] Geometrical specific area calculated by assuming all crystallites are spherical, $S_{geo} = 6/(\rho \cdot d)$. [d] Specific surface area and total pore volume obtained from N_2 adsorption isotherms.

Figure 1a gives the XRD patterns of the cobalt oxide catalysts calcined under different conditions. The diffraction peaks of all catalysts were well indexed to those of Co_3O_4 in the cubic spinel phase (a = 8.084 Å, Joint Committee on Powder Diffraction Standards (JCPDS), Card No. 74-2102). A higher calcination temperature led to sharper and stronger diffraction peaks due to the better crystallization of Co_3O_4. Meanwhile, calcination in dynamic air was conducive to obtaining broad and weak diffraction peaks. The average crystallite size(d), lattice constant(a), and strain of the catalysts were estimated by software MDI Jade 6.0 (Table 1). As expected, increasing the calcination temperature resulted in the sintering of Co_3O_4 crystallite, shrinkage of the Co_3O_4 lattice, and reduction in strain. The same trend was also observed when changing the calcination atmosphere from static air to dynamic air. Compared to other catalysts, smaller crystallite size, larger lattice constant, and more strain were observed for Co-350D, indicating the presence of more oxygen vacancies, point, or dislocation defects [39].

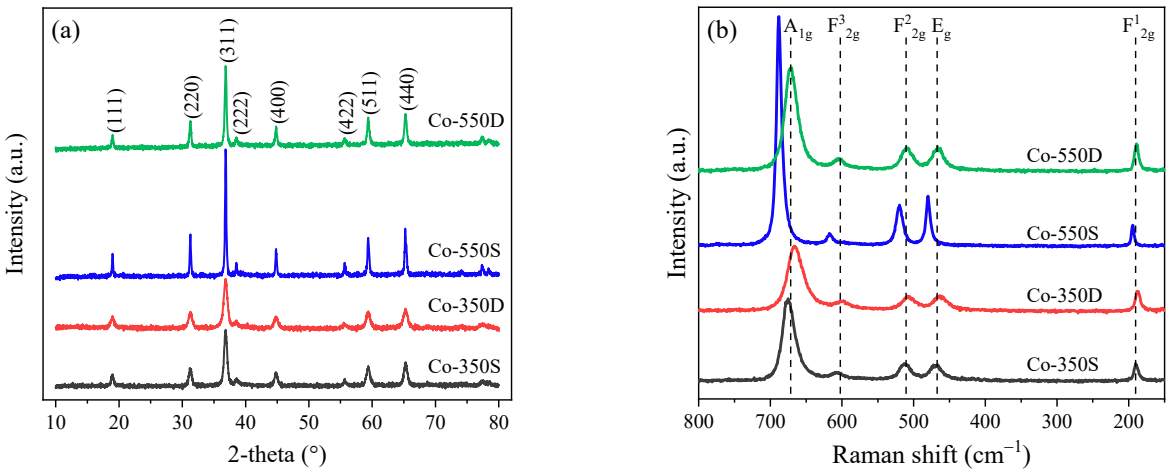

Figure 1. (**a**) XRD patterns and (**b**) Raman spectra of the Co_3O_4 catalysts calcined under different conditions.

Raman spectra were obtained to further study the lattice distortion of the Co_3O_4 catalysts. As displayed in Figure 1b, five Raman peaks correspond to A_{1g}, $F^3{}_{2g}$, $F^2{}_{2g}$, E_g, and $F^1{}_{2g}$ symmetries can be seen for all catalysts [18,40,41]. The calcination condition has a significant effect on the Raman spectra of Co_3O_4. For example, the peak positions of A_{1g} symmetry in all catalysts follow the order Co-350D (667 cm^{-1}) < Co-550D (670 cm^{-1}) < Co-350S (675 cm^{-1}) < Co-550S (688 cm^{-1}). The full width at half-maximum (FWHM) of A_{1g} symmetry decreases in the same order (Table 2). Thus, more defects caused by lattice distortion or residual stress of spinel crystal were present in Co_3O_4 catalysts calcined at low temperatures or under dynamic air [18], in line with the XRD analysis. In addition, the peak area ratios of $F^1{}_{2g}/A_{1g}$ (tetrahedral Co^{3+}–O^{2-}/octahedral Co^{2+}–O^{2-} [40]) were

calculated and summarized in Table 2. The results demonstrated that Co-350D possessed the highest concentration of Co^{2+} and oxygen defects [24].

Table 2. Quantitative analysis of Raman spectra and CO-TPR of the Co_3O_4 catalysts calcined under different conditions.

Catalysts	Raman Spectra			CO_2 Production in CO-TPR (mmol g^{-1})	
	Peak Position of A_{1g} (cm^{-1})	FWHM of A_{1g}	Peak Ratios of $F^1{}_{2g}/A_{1g}$	100–300 °C	Total
Co-350S	675	24	0.073	3.3	16.2
Co-350D	667	31	0.099	4.7	16.1
Co-550S	688	11	0.036	1.5	16.7
Co-550D	670	25	0.089	2.0	17.0

Figure 2 compares the N_2 adsorption-desorption isotherms and pore size distribution curves of the Co_3O_4 catalysts calcined under different conditions. Typical H3-type hysteresis loops due to capillary condensation in mesopores were observed and decreased in the order Co-350D > Co-350S > Co-550D > Co-550S. The calculated specific surface area and total pore volume follow the same tendency (Table 1). By assuming that all Co_3O_4 crystallites are spherical, the geometrical surface area of the catalysts was also estimated based on the XRD result (Table 1). The geometrical values are close to the SSA ones, implying that the Co_3O_4 nanoparticles are well dispersed without obvious aggregation. Regarding the pore size distribution, mesopores centered at ca. 19 and 31 nm were observed for Co-350D and Co-350S, respectively, whereas few mesopores can be seen for Co-550D and Co-550S. The results suggested that the Co_3O_4 catalysts suffered evident sintering when calcined at a higher temperature. Co-350D has the largest surface area (81 m^2 g^{-1}) and pore volume (0.365 cm^3 g^{-1}), which can be beneficial to the adsorption of reactants, exposure of active sites, and diffusion of reaction products.

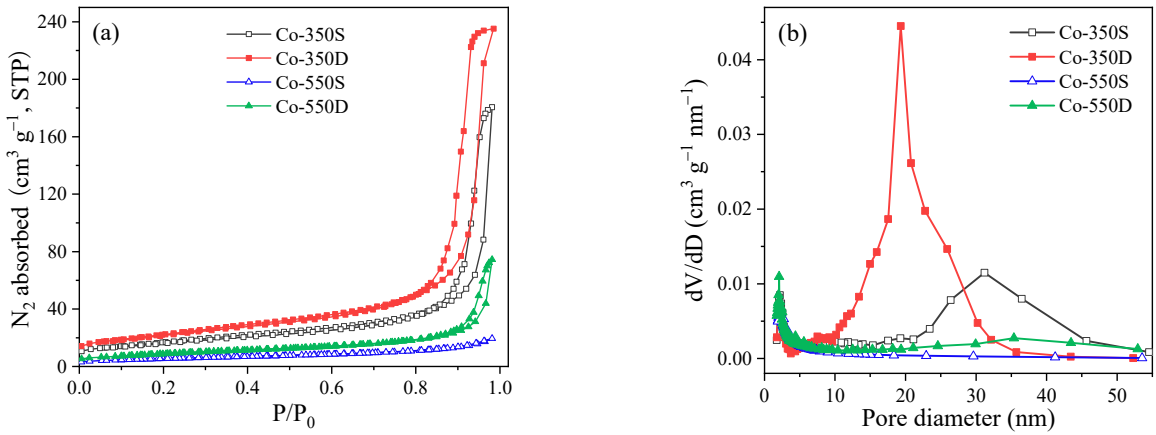

Figure 2. (**a**) N_2 adsorption–desorption isotherms and (**b**) pore size distribution curves of Co_3O_4 catalysts calcined under different conditions.

2.2. Reducibility

The reducibility of the as-prepared Co_3O_4 catalysts was investigated by CO-TPR, with the corresponding profiles shown in Figure 3. The CO_2 production curve matched perfectly with the CO consumption curve. The reduction of Co_3O_4 proceeds via two steps, the low-temperature peak was ascribed to $Co^{3+}\rightarrow Co^{2+}$ and the higher one $Co^{2+}\rightarrow Co^0$ [42], with total CO_2 production quantities of 16.1–17.0 mmol g^{-1} (Table 2). By comparing the low-temperature reduction peaks, the reducibility of the catalysts is ranked as Co-350D > Co-350S > Co-550D > Co-550S. Meanwhile, the CO_2 production amount in 100–300 °C of each catalyst was calculated (Table 2). The result further revealed the best low-temperature

reducibility of Co-350D, which may be related to its smallest crystallite size that can expose more reducible sites [14,24].

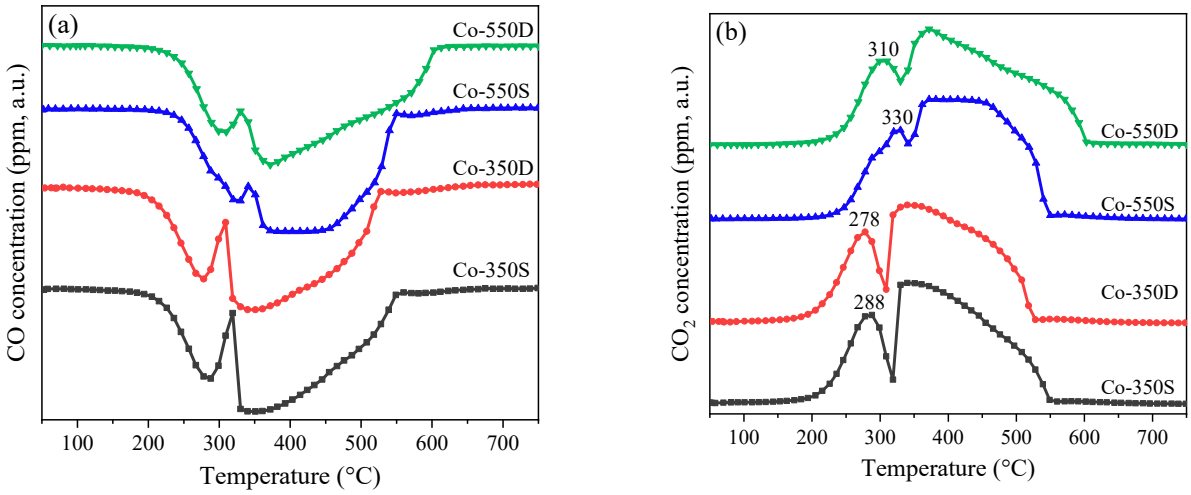

Figure 3. (**a**) CO consumption and (**b**) CO_2 production in CO-TPR profiles of the Co_3O_4 catalysts calcined under different conditions.

2.3. Catalytic Performance

The catalytic performance of the Co_3O_4 catalysts calcined in different conditions was evaluated in the total oxidation of toluene and propane, as presented in Figure 4. The reaction temperatures required for 10%, 50%, and 90% VOCs conversion (T_{10}, T_{50}, and T_{90}) were summarized in Table S1 to conveniently compare the catalytic performance. In terms of toluene oxidation, a significant difference in catalytic performance was observed in the low-temperature region. On the one hand, Co_3O_4 calcined at 350 °C performed much better than that calcined at 550 °C. On the other hand, Co_3O_4 calcined in dynamic air showed superior performance to that calcined in static air. The T_{10} value increased in the order of Co-350D > Co-350S > Co-550D > Co-550S. When the reaction temperature is higher than 240 °C, these catalysts behaved similarly in toluene oxidation. Regarding propane oxidation, the catalytic performance of these catalysts follows the same trend as that in toluene oxidation in the whole reaction temperature range. Co-350D exhibited the best performance whether in toluene or propane oxidation, which was further evidenced by the reaction rate vs temperature profiles (Figure S3).

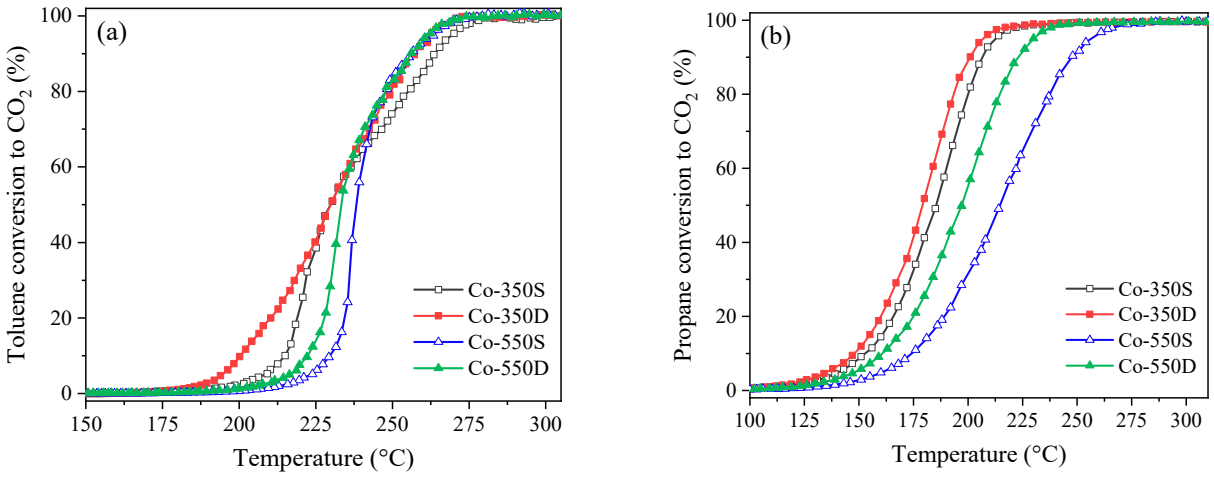

Figure 4. Light-off curves of (**a**) toluene and (**b**) propane oxidation over the Co_3O_4 catalysts calcined under different conditions.

The catalytic stability of the optimal catalyst Co-350D was studied by performing three consecutive catalytic cycles. As shown in Figure 5, the light-off curves of the three cycles were almost coincident, no matter in toluene or propane oxidation, suggesting the excellent cycling stability of the catalyst.

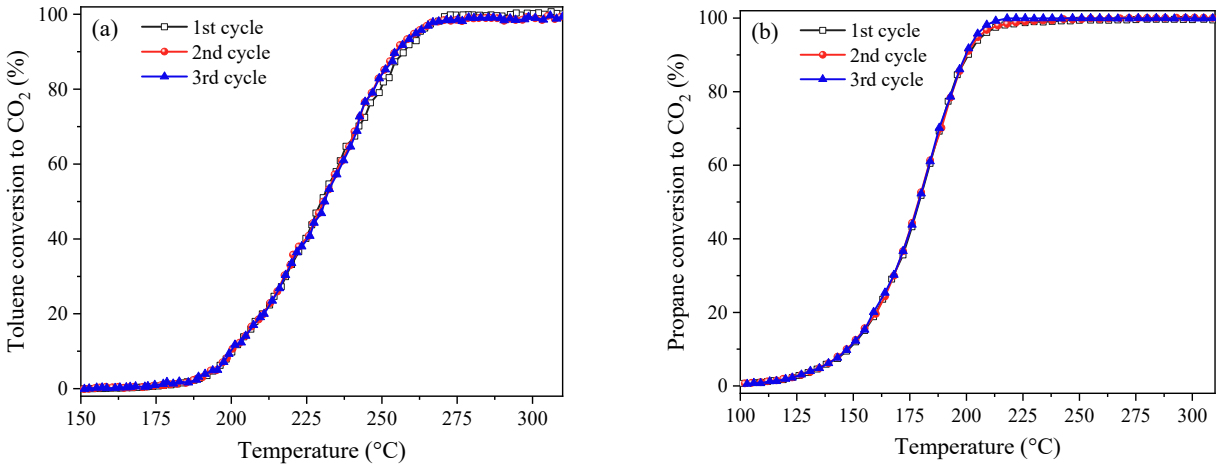

Figure 5. (**a**) Toluene and (**b**) propane conversion to CO_2 as a function of temperature over Co-350D upon three consecutive catalytic cooling cycles.

Furthermore, the long-term catalytic durability of Co-350D was investigated in toluene oxidation. As displayed in Figure 6a, in a continuous operation condition at 250 °C, toluene conversion to CO_2 first decreased from 80% to 40% in 3 h and then became wavy around 53% in the next 60 h. Once the toluene stream was removed, a large quantity of CO_2 was produced immediately, probably due to the fast decomposition of the accumulated reactive coke [43]. It has been previously reported that when the formation rate of reactive coke was faster than the reaction rate, these accumulated compounds would be quickly oxidized to induce self-heating of the catalyst, thus causing the oscillation phenomenon in the VOCs conversion into CO_2 [44]. After the catalyst was fully regenerated, the durability test was continued for another 20 h. A similar oscillation curve occurred again, indicating the reproducibility of the experimental result.

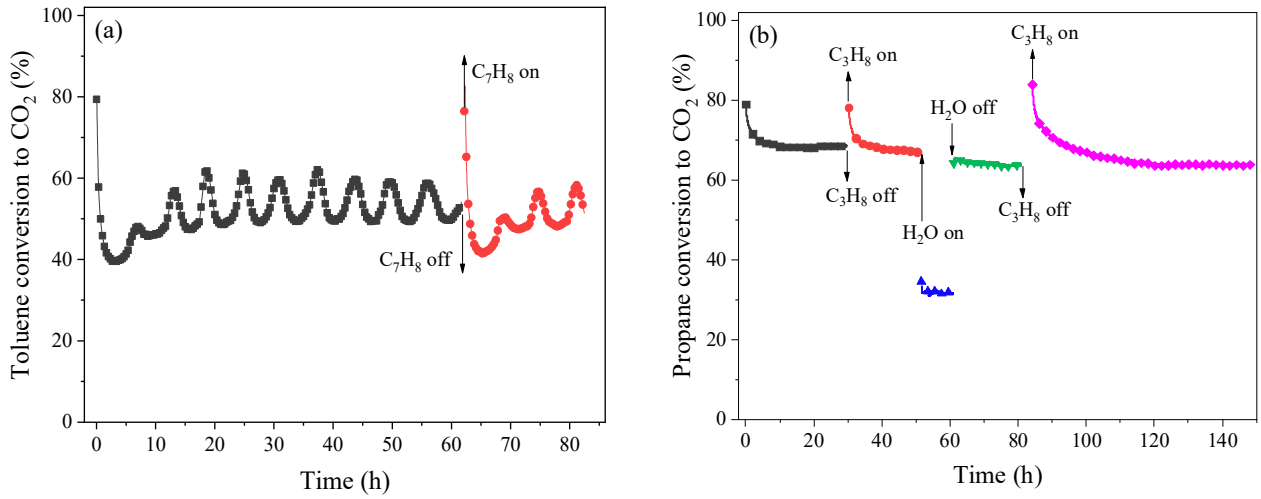

Figure 6. Long-term durability test over Co-350D in (**a**) toluene oxidation at 250 °C and (**b**) propane oxidation at 195 °C in the absence and presence of 4.4 vol.% H_2O.

Considering that water is always present in the catalytic oxidation process, either from the inlet gas or as a combustion product, the effect of water during the long-term durability

test in propane oxidation over Co-350D was investigated. Figure 6b shows the evolution of propane conversion to CO_2 as a function of time-on-stream at 195 °C over Co-350D in normal conditions or under water vapor-rich conditions (~4.4 vol.%). In dry gas, the initial propane conversion to CO_2 was ca. 80%, and it dropped up to 68% in 30 h. After the catalyst was reactivated by cutting off the propane stream, the conversion was back to the original level and declined to 68% again in the next 20 h. Then, 4.4 vol.% moisture was sent to the feed gas stream, causing a decrease in conversion to 32%, which can be a result of the blocking of active sites [45] or the shift of reaction equilibrium [46]. After operating in water vapor for 10 h, water vapor was removed, the conversion was recovered to 64% and maintained at this value for 20 h. Finally, the activity of the catalyst was restored again by stopping the propane stream and was reduced to 64% in the final 65 h. To conclude, in 150 h of testing in propane oxidation, Co-350D exhibited considerable stability and tolerance to water vapor. The deactivation of the catalyst was reversible.

The characterization and catalytic test results indicated that the calcination condition played a crucial role in tuning the properties of the Co_3O_4 catalysts and in turn, affected the catalytic activity. As shown in Figure 7a, there is a proportional relationship between the VOCs reaction rate of the Co_3O_4 catalysts and their low-temperature reducibility. Similarly, the catalytic activity is closely related to the strain of the catalyst (Figure 7b). Calcination at lower temperatures and/or in dynamic air is an effective way to enhance the activity of the Co_3O_4 catalysts. The Co_3O_4 catalyst calcined at 350 °C in dynamic air has the most defective structure, the largest SSA, and the best reducibility. As a result, Co-350D is the most active catalyst in the total oxidation of both toluene and propane.

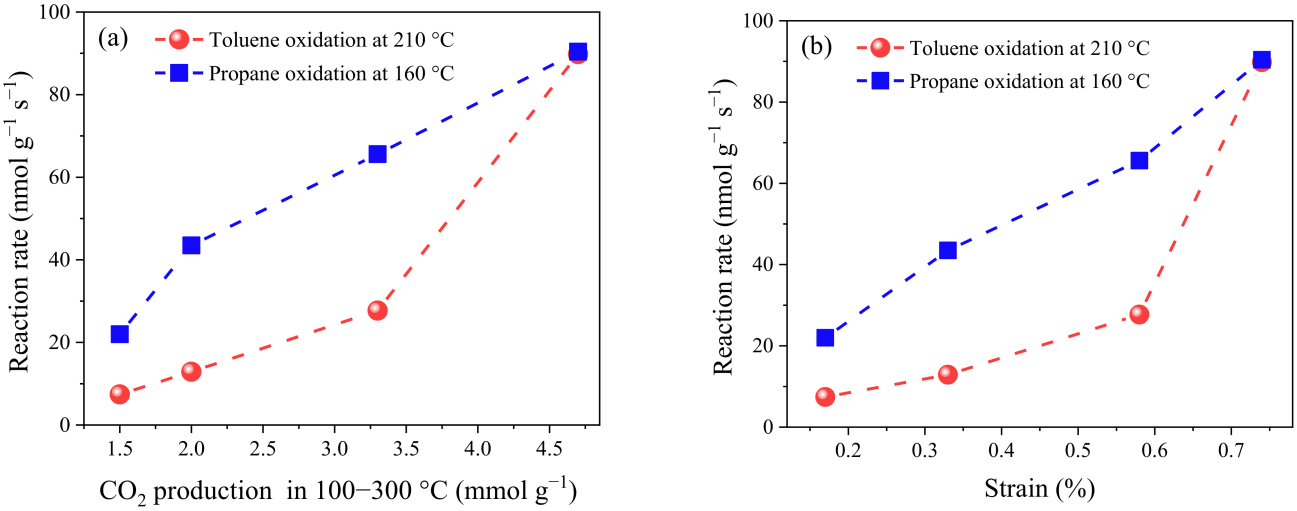

Figure 7. Correlation of (**a**) CO_2 production in 100–300 °C in CO-TPR and (**b**) the strain with toluene and propane oxidation rate over the Co_3O_4 catalysts.

Table 3 summarized the catalytic performance of typical Co_3O_4 catalysts reported by other authors in order to compare them with the as-prepared Co-350D. As we can see, in terms of toluene oxidation, Co-350D exhibits similar performance to Co_3O_4-HA [3], hydrangea-like Co_3O_4 microsphere [4], Co_3O_4-cube [5], and Co_3O_4-S-160 [6], whereas it is inferior to Co_3O_4-0.01 [7], 3D-Co_3O_4 [8], Co_3O_4–PTA–L2 [9], N-Co_3O_4-200 [10], and $Co_{3-x}O_{4-y}$ [11]. Nevertheless, it should be kept in mind that the T_{50} and T_{90} values used in this work are actually CO_2 yield, which has been previously emphasized to require a higher temperature than toluene conversion [46]. The total oxidation of toluene is a two-step process containing the oxidation of toluene to some intermediates (benzyl alcohol, benzaldehyde, and benzene) at low temperatures and further oxidation of these intermediates to CO_2 at higher temperatures [6]. Thus, the performance of Co-350D in toluene oxidation may be underrated. Moreover, the Co_3O_4 catalysts that performed better than Co-350D were mostly prepared by hydrothermal or hard-templating methods, using

surfactants, and consuming much energy. Regarding propane oxidation, it is clear that Co-350D precedes Co_3O_4-C100–550 [12], C-350 [13], CoDP [14], Co_3O_4-H [15], Mic-Co_3O_4 [16], Co_3O_4-AC [18] Co_4Zr_1 [19], and Ca-Co_3O_4-Ac [20], while it keeps pace with Co-SAS 10% water [17]. The comparison results further proved the superiority of Co-350D in the total oxidation of toluene and propane.

Table 3. Comparison of the catalytic performance in toluene and propane oxidation over various catalysts.

	Catalyst	WHSV (mL h^{-1} g^{-1})	VOC Content (vol.%)	T_{50}/T_{90}	Ref.
Toluene oxidation	Co_3O_4-HA	40,000	0.1	232/240	[3]
	Co_3O_4 microsphere	60,000	0.05	243/248	[4]
	Co_3O_4-cube	48,000	0.1	240/248	[5]
	Co_3O_4-S-160	60,000	0.05	236/250	[6]
	Co_3O_4-0.01	15,000	0.1	217/226	[7]
	3D-Co_3O_4	48,000	0.1	229/238	[8]
	Co_3O_4–PTA–L2	30,000	0.3	182/188	[9]
	N-Co_3O_4-200	60,000	0.1	208/218	[10]
	$Co_{3-x}O_{4-y}$	72,000	0.03	171/180	[11]
	Co-350D	40,000	0.1	230/257	This work
Propane oxidation	Co_3O_4-C100–550	12,000	0.8	200/213	[12]
	C-350	12,000	0.8	210/235	[13]
	CoDP	120,000	0.1	195/225	[14]
	Co_3O_4-H	9990	1.0	209/239	[15]
	Mic-Co_3O_4	120,000	0.8	262/374	[16]
	Co-SAS 10% water	15,000	0.5	175/200	[17]
	Co_3O_4-AC	240,000	0.3	237/250	[18]
	Co_4Zr_1	60,000	0.2	210/242	[19]
	Ca-Co_3O_4-Ac	120,000	0.2	236/260	[20]
	Co-350D	40,000	0.1	180/201	This work

3. Experimental

3.1. Catalyst Preparation

Two hundred mL of 0.4 M $Co(NO_3)_2 \cdot 6H_2O$ solution was mixed with 200 mL of 0.44 M Na_2CO_3 solution under vigorous stirring. Meanwhile, the pH of the mixture was adjusted to 9.5 by Na_2CO_3 solution and maintained at this value for 1 h. The obtained slurry was centrifuged and washed several times with distilled water. After drying at 80 °C overnight, the powder was divided into four parts. Two of them were calcined at 350 or 550 °C (2 °C min^{-1}) for 2 h in static air, and the other two were calcined at 350 or 550 °C (2 °C min^{-1}) for 2 h in dynamic air with a flow rate of 100 mL min^{-1}. For facile description, the as-prepared four samples were referred to as Co-350S, Co-350D, Co-550S, and Co-550D, respectively, where S represents static air calcination and D represents dynamic air calcination.

3.2. Catalyst Characterization

Thermogravimetry and differential thermal analysis (TG/DTA) experiments were carried out using a Setsys Evolution 12 calorimeter (SETARAM, Lyon, France). The cobalt precursor was heated from 25 to 800 °C at 10 °C min^{-1} in an air stream.

Fourier Transform infrared (FTIR) spectra were obtained using a FT-IR C92712 spectrometer (PerkinElmer, Waltham, MA, USA) in an attenuated total reflectance mode from 4000 to 400 cm^{-1}.

The chemical composition of the cobalt oxides was measured using inductively coupled plasma optical emission spectroscopy (ICP-OES, Horiba Jobin Yvon, Paris, France). Prior to measurement, the powder was dissolved in a mixture solution of H_2SO_4 and HNO_3 at ca. 400 °C.

X-ray diffraction (XRD) patterns were recorded using a D8 Advance diffractometer (Bruker, Karlsruhe, Germany) with Cu Kα radiation (λ = 0.154184 nm). Samples were scanned from 10° < 2θ < 80° with a step of 0.02° and counting time of 2 s per step.

Raman spectra were collected using a LabRam HR spectrometer (Horiba, Paris, France) with an Ar^+ laser beam (λ = 514 nm) from 800 to 150 cm^{-1}.

N_2 adsorption–desorption isotherms were determined at −196 °C using a TRISTAR II apparatus (Micromeritics, Norcross, GA, USA). The samples were pre-degassed at 300 °C for 3 h. The specific surface area was calculated by the standard Brunauer–Emmett–Teller (BET) method, and the total pore volume and pore size distribution were obtained using the Barrett–Joyner–Halenda (BJH) method.

Temperature program reduction in CO (CO-TPR) was performed using a Micro-GC (SRA % GC-R3000, SRA Instruments, Milan, Italy). Typically, 0.03 g of the sample was pretreated in pure He at 300 °C for 0.5 h and then cooled down to 50 °C. The reduction experiment was performed in 0.3 vol.% CO/He gas mixture (100 mL min^{-1}), from 50 to 750 °C at 5 °C min^{-1}.

3.3. Catalytic Test

The catalytic test was performed in a U-shaped quartz reactor (i.d. = 4 mm). In each test, 0.15 g of catalyst was mixed with ca. 0.7 g of silicon carbide to avoid hot spot and maintain a catalytic bed height of 6 mm. The total flow rate was controlled at 100 mL min^{-1}, corresponding to a weight hourly space velocity (WHSV) of 40,000 mL g^{-1} h^{-1}.

The reaction temperature program for toluene and propane oxidation was shown in Schematic S1. In toluene oxidation, T = 150 °C, the feed gas was composed of 1000 ppm of toluene and 21 vol.% O_2 balanced by N_2. The concentrations of CO and CO_2 were monitored using an online Rosemount Stream Gas Infrared Analyzer (Emerson Electric Co., St. Louis, MO, USA). In propane oxidation, T = 100 °C, the feed gas was composed of 1000 ppm of propane and 21 vol.% O_2 balanced by He. An online micro gas chromatograph (SRA % GC-R3000) equipped with two thermal conductivity detectors was used to monitor the gas effluents. The light-off curves during the cooling ramp were used to compare the catalytic performance.

The conversion of toluene/propane to CO_2 was calculated as follows (Equations (1) and (2)):

$$X_{C_7H_8}(\%) = \frac{[CO_2]}{7[C_7H_8]} \times 100 \quad (1)$$

$$X_{C_3H_8}(\%) = \frac{[CO_2]}{3[C_3H_8]} \times 100 \quad (2)$$

where $[CO_2]$, $[C_7H_8]$, and $[C_3H_8]$ represent the outlet CO_2 concentration, the inlet toluene, and propane concentration, respectively.

The toluene/propane oxidation reaction rate (r, mol s^{-1} g^{-1}) was calculated as follows (Equation (3)):

$$r = \frac{X \cdot F}{m} \quad (3)$$

where X is the conversion of toluene/propane to CO_2, F is the flow rate of toluene/propane (mol s^{-1}) in the inlet gas, and m is the mass of the catalyst used (g).

4. Conclusions

In this study, different calcination conditions were applied to optimize the structural and textural properties of Co_3O_4 catalysts synthesized by carbonate precipitating at pH 9.5. The as-prepared catalysts exhibited high activity in the total oxidation of toluene and propane. Among them, the catalyst calcined at 350 °C under dynamic air (Co-350D) performed much better, with T_{90} values of 257 and 201 °C in the toluene or propane oxidation, respectively. The superior catalytic performances of Co-350D could be attributed to their smaller crystallite size, larger surface area, abundant surface Co^{2+}species, and good

reducibility. Co-350D showed impressive cycling stability, whereas it deactivated slightly upon long-term durability tests due to the accumulation of reaction intermediates on the catalyst surface. In addition, propane oxidation over Co-350D appeared to be inhibited by the presence of 4.4 vol.% H_2O and the observed deactivation was reversible.

Supplementary Materials: The following supporting information can be downloaded at: https://www.mdpi.com/article/10.3390/catal13060992/s1, Table S1: Light-off temperatures at 10, 50, and 90% conversion (T_{10}, T_{50}, and T_{90}, respectively) of toluene/propane to CO_2; Schematic S1: Reaction temperature program used in catalytic test. Figure S1: TG weight loss curve of the 80 °C dried cobalt precursor; Figure S2: FTIR spectra of the cobalt precursor and the Co_3O_4 catalysts calcined under different conditions; Figure S3: (a) Toluene and (b) propane oxidation rate as a function of temperature over the Co_3O_4 catalysts calcined under different conditions.

Author Contributions: This work was completed jointly by all authors. W.Z. prepared the catalysts, performed structural characterizations, conducted catalytic oxidation tests, and wrote the manuscript. W.Z., C.D., J.L.V. and A.G.-F. coordinated the whole study, including data interpretation, result discussion, and manuscript review and revision. All authors have read and agreed to the published version of the manuscript.

Funding: This research received no external funding.

Data Availability Statement: Available upon request.

Acknowledgments: This work was financially supported by Anhui University of Technology, Université Claude Bernard Lyon 1, University of Castilla-La Mancha and CNRS.

Conflicts of Interest: The authors declare no conflict of interest.

References

1. Guo, Y.; Wen, M.; Li, G.; An, T. Recent advances in VOC elimination by catalytic oxidation technology onto various nanoparticles catalysts: A critical review. *Appl. Catal. B Environ.* **2021**, *281*, 119447. [CrossRef]
2. Liotta, L.F. Catalytic oxidation of volatile organic compounds on supported noble metals. *Appl. Catal. B Environ.* **2010**, *100*, 403–412. [CrossRef]
3. Shen, Y.; Deng, J.; Impeng, S.; Li, S.; Yan, T.; Zhang, J.; Shi, L.; Zhang, D. Boosting toluene combustion by engineering Co–O strength in cobalt oxide catalysts. *Environ. Sci. Technol.* **2020**, *54*, 10342–10350. [CrossRef] [PubMed]
4. Liu, W.; Liu, R.; Zhang, H.; Jin, Q.; Song, Z.; Zhang, X. Fabrication of Co_3O_4 nanospheres and their catalytic performances for toluene oxidation: The distinct effects of morphology and oxygen species. *Appl. Catal. A Gen.* **2020**, *597*, 117539. [CrossRef]
5. Ren, Q.; Mo, S.; Peng, R.; Feng, Z.; Zhang, M.; Chen, L.; Fu, M.; Wu, J.; Ye, D. Controllable synthesis of 3D hierarchical Co_3O_4 nanocatalysts with various morphologies for the catalytic oxidation of toluene. *J. Mater. Chem. A* **2018**, *6*, 498–509. [CrossRef]
6. Liu, W.; Liu, R.; Zhang, X. Controllable synthesis of 3D hierarchical Co_3O_4 catalysts and their excellent catalytic performance for toluene combustion. *Appl. Surf. Sci.* **2020**, *507*, 145174. [CrossRef]
7. Li, G.; Zhang, C.; Wang, Z.; Huang, H.; Peng, H.; Li, X. Fabrication of mesoporous Co_3O_4 oxides by acid treatment and their catalytic performances for toluene oxidation. *Appl. Catal. A Gen.* **2018**, *550*, 67–76. [CrossRef]
8. Ren, Q.; Feng, Z.; Mo, S.; Huang, C.; Li, S.; Zhang, W.; Chen, L.; Fu, M.; Wu, J.; Ye, D. 1D-Co_3O_4, 2D-Co_3O_4, 3D-Co_3O_4 for catalytic oxidation of toluene. *Catal. Today* **2019**, *332*, 160–167. [CrossRef]
9. Han, W.; Tang, Z.; Lin, Q. Morphology-controlled synthesis of the metal–organic framework-derived nanorod interweaved lamellose structure Co_3O_4 for outstanding catalytic combustion performance. *Cryst. Growth Des.* **2019**, *19*, 4546–4556. [CrossRef]
10. Bao, L.; Zhu, S.; Chen, Y.; Wang, Y.; Meng, W.; Xu, S.; Lin, Z.; Li, X.; Sun, M.; Guo, L. Anionic defects engineering of Co_3O_4 catalyst for toluene oxidation. *Fuel* **2022**, *314*, 122774. [CrossRef]
11. Li, Y.; Chen, T.; Zhao, S.; Wu, P.; Chong, Y.; Li, A.; Zhao, Y.; Chen, G.; Jin, X.; Qiu, Y.; et al. Engineering cobalt oxide with coexisting cobalt defects and oxygen vacancies for enhanced catalytic oxidation of toluene. *ACS Catal.* **2022**, *12*, 4906–4917. [CrossRef]
12. Garcia, T.; Agouram, S.; Sánchez-Royo, J.F.; Murillo, R.; Mastral, A.M.; Aranda, A.; Vázquez, I.; Dejoz, A.; Solsona, B. Deep oxidation of volatile organic compounds using ordered cobalt oxides prepared by a nanocasting route. *Appl. Catal. A Gen.* **2010**, *386*, 16–27. [CrossRef]
13. Puértolas, B.; Smith, A.; Vázquez, I.; Dejoz, A.; Moragues, A.; Garcia, T.; Solsona, B. The different catalytic behaviour in the propane total oxidation of cobalt and manganese oxides prepared by a wet combustion procedure. *Chem. Eng. J.* **2013**, *229*, 547–558. [CrossRef]
14. Zhang, W.; Wu, F.; Li, J.; You, Z. Dispersion–precipitation synthesis of highly active nanosized Co_3O_4 for catalytic oxidation of carbon monoxide and propane. *Appl. Surf. Sci.* **2017**, *411*, 136–143. [CrossRef]
15. Yao, J.; Shi, H.; Sun, D.; Lu, H.; Hou, B.; Jia, L.; Xiao, Y.; Li, D. Facet-dependent activity of Co_3O_4 catalyst for C_3H_8 combustion. *ChemCatChem* **2019**, *11*, 5570–5579. [CrossRef]

16. Lin, D.; Zheng, Y.; Feng, X.; You, Y.; Wu, E.; Luo, Y.; Qian, Q.; Chen, Q. Highly stable Co_3O_4 nanoparticles-assembled microrods derived from MOF for efficient total propane oxidation. *J. Mater. Sci.* **2020**, *55*, 5190–5202. [CrossRef]
17. Marin, R.P.; Kondrat, S.A.; Pinnell, R.K.; Davies, T.E.; Golunski, S.; Bartley, J.K.; Hutchings, G.J.; Taylor, S.H. Green preparation of transition metal oxide catalysts using supercritical CO_2 anti-solvent precipitation for the total oxidation of propane. *Appl. Catal. B Environ.* **2013**, *140–141*, 671–679. [CrossRef]
18. Tang, W.; Xiao, W.; Wang, S.; Ren, Z.; Ding, J.; Gao, P.-X. Boosting catalytic propane oxidation over PGM-free Co_3O_4 nanocrystal aggregates through chemical leaching: A comparative study with Pt and Pd based catalysts. *Appl. Catal. B Environ.* **2018**, *226*, 585–595. [CrossRef]
19. He, C.; Ao, C.; Ruan, S.; Xu, K.; Zhang, L. Catalytic combustion of propane over Zr-modified Co_3O_4 catalysts: An experimental and theoretical study. *Colloids Surf. A Physicochem. Eng. Asp.* **2022**, *641*, 128617. [CrossRef]
20. Zhu, W.; Wang, X.; Li, C.; Chen, X.; Li, W.; Liu, Z.; Liang, C. Defect engineering over Co_3O_4 catalyst for surface lattice oxygen activation and boosted propane total oxidation. *J. Catal.* **2022**, *413*, 150–162. [CrossRef]
21. Liotta, L.F.; Wu, H.; Pantaleo, G.; Venezia, A.M. Co3O4 nanocrystals and Co_3O_4–MOx binary oxides for CO, CH_4 and VOC oxidation at low temperatures: A review. *Catal. Sci. Technol.* **2013**, *3*, 3085. [CrossRef]
22. Fan, Z.; Zhang, Z.; Fang, W.; Yao, X.; Zou, G.; Shangguan, W. Low-temperature catalytic oxidation of formaldehyde over Co_3O_4 catalysts prepared using various precipitants. *Chin. J. Catal.* **2016**, *37*, 947–954. [CrossRef]
23. Zheng, Y.; Liu, Y.; Zhou, H.; Huang, W.; Pu, Z. Complete combustion of methane over Co_3O_4 catalysts: Influence of pH values. *J. Alloys Compd.* **2018**, *734*, 112–120. [CrossRef]
24. De Rivas, B.; López-Fonseca, R.; Jiménez-González, C.; Gutiérrez-Ortiz, J.I. Synthesis, characterisation and catalytic performance of nanocrystalline Co_3O_4 for gas-phase chlorinated VOC abatement. *J. Catal.* **2011**, *281*, 88–97. [CrossRef]
25. Dissanayake, S.; Wasalathanthri, N.; Shirazi Amin, A.; He, J.; Poges, S.; Rathnayake, D.; Suib, S.L. Mesoporous Co_3O_4 catalysts for VOC elimination: Oxidation of 2-propanol. *Appl. Catal. A Gen.* **2020**, *590*, 117366. [CrossRef]
26. Zhang, W.; Díez-Ramírez, J.; Anguita, P.; Descorme, C.; Valverde, J.L.; Giroir-Fendler, A. Nanocrystalline Co_3O_4 catalysts for toluene and propane oxidation: Effect of the precipitation agent. *Appl. Catal. B Environ.* **2020**, *273*, 118894. [CrossRef]
27. Zhang, W.; Lassen, K.; Descorme, C.; Valverde, J.L.; Giroir-Fendler, A. Effect of the precipitation pH on the characteristics and performance of Co_3O_4 catalysts in the total oxidation of toluene and propane. *Appl. Catal. B Environ.* **2021**, *282*, 119566. [CrossRef]
28. Chen, H.; Liu, P.; Wei, G.; Huang, Y.; Lin, X.; Liang, X.; Zhu, J. Effect of electron structure on the catalytic activity of $LaCoO_3$ perovskite towards toluene oxidation. *Chem. Commun.* **2022**, *58*, 4731–4734. [CrossRef]
29. Li, J.B.; Jiang, Z.Q.; Qian, K.; Huang, W.X. Effect of calcination temperature on surface oxygen vacancies and catalytic performance towards CO oxidation of Co_3O_4 nanoparticles supported on SiO_2. *Chin. J. Chem. Phys.* **2012**, *25*, 103–109. [CrossRef]
30. Wang, M.; Qi, L.; Li, X. Modulating defective oxygen of Co-based crystals by calcination temperature control for improving the catalytic removal of propane. *CrystEngComm* **2022**, *24*, 7902–7905. [CrossRef]
31. Liu, Z.G.; Chai, S.H.; Binder, A.; Li, Y.Y.; Ji, L.T.; Dai, S. Influence of calcination temperature on the structure and catalytic performance of CuO_x-CoO_y-CeO_2 ternary mixed oxide for CO oxidation. *Appl. Catal. A Gen.* **2013**, *451*, 282–288. [CrossRef]
32. Wu, H.; Pantaleo, G.; Di Carlo, G.; Guo, S.; Marcì, G.; Concepción, P.; Venezia, A.M.; Liotta, L.F. Co_3O_4 particles grown over nanocrystalline CeO_2: Influence of precipitation agents and calcination temperature on the catalytic activity for methane oxidation. *Catal. Sci. Technol.* **2015**, *5*, 1888–1901. [CrossRef]
33. Li, H.; Lu, G.; Qiao, D.; Wang, Y.; Guo, Y.; Guo, Y. Catalytic methane combustion over Co_3O_4/CeO_2 composite oxides prepared by modified citrate sol–gel method. *Catal. Lett.* **2011**, *141*, 452–458. [CrossRef]
34. Onrubia, J.A.; Pereda-Ayo, B.; De-La-Torre, U.; González-Velasco, J.R. Key factors in Sr-doped $LaBO_3$ (B = Co or Mn) perovskites for NO oxidation in efficient diesel exhaust purification. *Appl. Catal. B Environ.* **2017**, *213*, 198–210. [CrossRef]
35. Klissurski, D.; Uzunova, E. Synthesis of nickel cobaltite spinel from coprecipitated nickel-cobalt hydroxide carbonate. *Chem. Mater.* **1991**, *3*, 1060–1063. [CrossRef]
36. Xu, R.; Zeng, H.C. Dimensional control of cobalt-hydroxide-carbonate nanorods and their thermal conversion to one-dimensional arrays of Co_3O_4 nanoparticles. *J. Phys. Chem. B* **2003**, *107*, 12643–12649. [CrossRef]
37. Wang, Y.; Lei, Y.; Li, J.; Gu, L.; Yuan, H.; Xiao, D. Synthesis of 3D-nanonet hollow structured Co_3O_4 for high capacity supercapacitor. *ACS Appl. Mater. Interfaces* **2014**, *6*, 6739–6747. [CrossRef]
38. Yan, Q.; Li, X.; Zhao, Q.; Chen, G. Shape-controlled fabrication of the porous Co_3O_4 nanoflower clusters for efficient catalytic oxidation of gaseous toluene. *J. Hazard. Mater.* **2012**, *209–210*, 385–391. [CrossRef]
39. Liu, Q.; Wang, L.-C.C.; Chen, M.; Cao, Y.; He, H.-Y.Y.; Fan, K.-N.N. Dry citrate-precursor synthesized nanocrystalline cobalt oxide as highly active catalyst for total oxidation of propane. *J. Catal.* **2009**, *263*, 104–113. [CrossRef]
40. Lou, Y.; Ma, J.; Cao, X.; Wang, L.; Dai, Q.; Zhao, Z.; Cai, Y.; Zhan, W.; Guo, Y.Y.; Hu, P.; et al. Promoting effects of In_2O_3 on Co_3O_4 for CO oxidation: Tuning O_2 activation and CO adsorption strength simultaneously. *ACS Catal.* **2014**, *4*, 4143–4152. [CrossRef]
41. González-Prior, J.; López-Fonseca, R.; Gutiérrez-Ortiz, J.I.I.; de Rivas, B. Oxidation of 1,2-dichloroethane over nanocube-shaped Co3O4 catalysts. *Appl. Catal. B Environ.* **2016**, *199*, 384–393. [CrossRef]
42. Tang, W.; Weng, J.; Lu, X.; Wen, L.; Suburamanian, A.; Nam, C.-Y.Y.; Gao, P.-X.X. Alkali-metal poisoning effect of total CO and propane oxidation over Co_3O_4 nanocatalysts. *Appl. Catal. B Environ.* **2019**, *256*, 117859. [CrossRef]
43. Genty, E.; Brunet, J.; Poupin, C.; Ojala, S.; Siffert, S.; Cousin, R. Influence of CO addition on the toluene total oxidation over Co based mixed oxide catalysts. *Appl. Catal. B Environ.* **2019**, *247*, 163–172. [CrossRef]

44. Tsou, J.; Magnoux, P.; Guisnet, M.; Órfão, J.J.M.; Figueiredo, J.L. Oscillations in the catalytic oxidation of volatile organic compounds. *J. Catal.* **2004**, *225*, 147–154. [CrossRef]
45. Zhu, W.; Chen, X.; Jin, J.; Di, X.; Liang, C.; Liu, Z. Insight into catalytic properties of Co_3O_4-CeO_2 binary oxides for propane total oxidation. *Chin. J. Catal.* **2020**, *41*, 679–690. [CrossRef]
46. Chen, J.; Chen, X.; Xu, W.; Xu, Z.; Chen, J.; Jia, H.; Chen, J. Hydrolysis driving redox reaction to synthesize Mn-Fe binary oxides as highly active catalysts for the removal of toluene. *Chem. Eng. J.* **2017**, *330*, 281–293. [CrossRef]

Disclaimer/Publisher's Note: The statements, opinions and data contained in all publications are solely those of the individual author(s) and contributor(s) and not of MDPI and/or the editor(s). MDPI and/or the editor(s) disclaim responsibility for any injury to people or property resulting from any ideas, methods, instructions or products referred to in the content.